Spectrochimica Acta Part B 76 (2012) 133–139

Contents lists available at SciVerse ScienceDirect

Spectrochimica Acta Part B

journal homepage: www.elsevier.com/locate/sab

Quantitative real-time monitoring of multi-elements in airborne particulates by direct introduction into an inductively coupled plasma mass spectrometer ☆

Yoshinari Suzuki, Hikaru Sato, Katsuhiro Hiyoshi, Naoki Furuta *

Faculty of Science and Engineering, Department of Applied Chemistry, Chuo University, 1-13-27, Kasuga, Bunkyo-ku, Tokyo 112-8551, Japan

ARTICLE INFO

Article history:
Received 16 May 2012
Accepted 11 June 2012
Available online 17 June 2012

Keywords:
Airborne particulates
Real-time monitoring
Metal oxides
Melting points
ICP-MS

ABSTRACT

A new calibration system for real-time determination of trace elements in airborne particulates was developed. Airborne particulates were directly introduced into an inductively coupled plasma mass spectrometer, and the concentrations of 15 trace elements were determined by means of an external calibration method. External standard solutions were nebulized by an ultrasonic nebulizer (USN) coupled with a desolvation system, and the resulting aerosol was introduced into the plasma. The efficiency of sample introduction via the USN was calculated by two methods: (1) the introduction of a Cr standard solution via the USN was compared with introduction of a $Cr(CO)_6$ standard gas via a standard gas generator and (2) the aerosol generated by the USN was trapped on filters and then analyzed. The Cr introduction efficiencies obtained by the two methods were the same, and the introduction efficiencies of the other elements were equal to the introduction efficiency of Cr. Our results indicated that our calibration method for introduction efficiency worked well for the 15 elements (Ti, V, Cr, Mn, Co, Ni, Cu, Zn, As, Mo, Sn, Sb, Ba, Tl and Pb). The real-time data and the filter-collection data agreed well for elements with low-melting oxides (V, Co, As, Mo, Sb, Tl, and Pb). In contrast, the real-time data were smaller than the filter-collection data for elements with high-melting oxides (Ti, Cr, Mn, Ni, Cu, Zn, Sn, and Ba). This result implies that the oxides of these 8 elements were not completely fused, vaporized, atomized, and ionized in the initial radiation zone of the inductively coupled plasma. However, quantitative real-time monitoring can be realized after correction for the element recoveries which can be calculated from the ratio of real-time data/filter-collection data.

1. Introduction

Multi-element analysis of airborne particulate matter is generally performed by means of inductively coupled plasma mass spectrometry (ICP-MS) or optical emission spectrometry after airborne particulates (APs) are collected on a filter and then dissolved by acid digestion [1–3]. However, obtaining enough APs for ICP-MS requires several hours or days, and thus the results provide average concentrations of elements in APs from various sources during the sampling period.

Trace elements in APs have been also measured online in real time by direct introduction of air samples into the spectrometer via a nebulizer [4–7]. However, the volume of the air sample is limited with this method. To increase the air sample volume, a differential mobility analyzer has been used as a gas-exchange device [8]. In addition, Nishiguchi et al. recently reported a gas-exchange device for ICP-MS that exchanges the gas molecules from air to Ar without any loss of particulate matter, and the resulting gas-converted air sample can be introduced directly into the ICP-MS instrument [9]. However, the multi-element data obtained by these investigators were only qualitative, although semi-quantitative data were obtained for Sn. In previous work, we reported the quantification of Pb in a single nanoparticle (diameter, 90 nm; mass, 0.458 fg) calibrated by an external standard introduced with an ultrasonic nebulizer (USN) coupled with a desolvator system [10], but this method has not yet been validated.

In this study, we evaluated the efficiency of sample introduction via the USN by collecting aerosols generated by the USN on filters and then analyzing the aerosols. Then, we calibrated real-time data by nebulizing an external multi-element standard solution and using the sample introduction efficiency of the USN. During real-time analysis, we also simultaneously collected APs on a filter, and we validated the real-time data by comparison with the filter-collection data.

2. Experimental

2.1. Reagents

A custom multi-element standard solution (Be, Al, V, Cr, Mn, Co, Ni, Cu, Zn, As, Se, Mo, Ag, Cd, Sb, Ba, Tl, Pb Th, and U) (XSTC-384, SPEX CertiPrep Inc., Metuchen, NJ) and Ti (PLTL9-2Y, SPEX CertiPrep Inc.) and Sn (PLSN2-2X, SPEX CertiPrep Inc.) standard solutions were used as an external standard for real-time analysis. A $Cr(CO)_6$

☆ This paper is dedicated to Gary M. Hieftje, on the occasion of his 70th birthday, in recognition of his boundless contributions to spectroscopy and analytical chemistry.

* Corresponding author.
E-mail address: nfuruta@chem.chuo-u.ac.jp (N. Furuta).

0584-8547/$ – see front matter © 2012 Elsevier B.V. All rights reserved.
doi:10.1016/j.sab.2012.06.001

gas, which was generated by standard gas generator (J-Science Lab Co., Kyoto, Japan), was used for the determination of the sample introduction efficiency of the USN. Nitric acid (70%, electronic laboratory grade, Kanto), HF (50%, semiconductor grade, Daikin Industries Co., Tokyo, Japan), H_2O_2 (30%, electronic laboratory grade, Kanto), and ultrapure water (Milli-Q Element, Millipore, Tokyo, Japan) were used for sample digestion and preparation of standard solutions.

2.2. System for real-time determination of elements in APs

A schematic diagram of the analytical apparatus is shown in Fig. 1. Outdoor air samples were collected from the rooftop (30 m high) of building no. 5 of Chuo University (Kasuga, Bunkyo-ku, Tokyo) through an 80-m-long Tygon tube (inside diameter is 7.94 mm) by means of a diaphragm pump equipped with a mass flow controller. The sampling dates are listed in Table 1. Additionally, a blank air sample was collected from a clean bench (class 100) equipped with HEPA filters. Each air sample was introduced to a multinozzle cascade impactor (inline type with NL-1-1A (<1.0 μm) or NL-1-2.5A (<2.5 μm), Tokyo Dylec Corp., Tokyo, Japan) at a flow rate of 1.0 L min^{-1}. A portion of the sample was vacuumed from the impactor at 0.75 L min^{-1} by means of a diaphragm pump equipped with a mass flow controller, and the APs from this portion were collected on a cellulose nitrate filter (VSWP04700; pore size, 0.025 μm; Millipore, Tokyo). The remaining portion of the flow (0.25 L min^{-1}) was introduced to a gas-exchange device (J-Science Lab Co., Kyoto, Japan), which replaced the air with Ar. This portion of the air sample was introduced to the ICP-MS (HP4500, Agilent Technologies, Tokyo, Japan) by means of a micro diaphragm gas-sampling pump (NMP05L, KNF Neuberger AG, Balterswil, Switzerland).

Standard $Cr(CO)_6$ gas was introduced to the ICP-MS via an Ar flow at 0.05 L min^{-1}. The multi-element standard solution was introduced to the ICP-MS via a USN coupled with a desolvation system (U6000AT+, CETAC, Omaha, NE, USA). Milli-Q water was continuously introduced via the USN/desolvation system during analysis of the $Cr(CO)_6$ standard gas as well as during tuning of the ICP-MS instrument and analysis of the air samples. The ICP-MS operating conditions are summarized in Table 1.

2.3. Calculation of USN sample introduction efficiency by comparison with introduction of $Cr(CO)_6$ by a standard gas generator

We calculated the sample introduction efficiency of the USN daily by comparing ^{53}Cr intensities measured by the ICP-MS for a standard $Cr(CO)_6$ gas with intensities measured for a Cr standard solution. A 5.0 ng mL^{-1} Cr standard solution was prepared by diluting 1000 μg mL^{-1} Cr with 0.1 mol L^{-1} nitric acid. The standard Cr solution was introduced to the USN at an uptake rate of 1.56 mL min^{-1}, and the resulting nebulized mist was dewatered by the desolvation system. The signal intensities of ^{53}Cr were measured 5 times over a sampling period of 9 s. When standard gases and solutions were analyzed, air samples were obtained from the clean bench. The introduction efficiency (E_g) of the Cr standard solution was calculated by means of the following equation:

$$E_g = \frac{F_g \times (I_s - I_b)}{C \times F_s (I_g - I_b)} \times 100\% \quad (1)$$

where F_g is the mass flow rate of the Cr as $Cr(CO)_6$ standard gas (ng min^{-1}) determined previously [10]; C is the Cr concentration (ng mL^{-1}) in the standard solution introduced into the USN; F_s is the uptake rate (mL min^{-1}) of the Cr standard solution into the USN; and I_s, I_g, and I_b are the ^{53}Cr intensities of the standard solution, the standard gas, and the blank, respectively.

2.4. Calculation of USN sample introduction efficiency by comparison with filter-collection data

A 200 ng mL^{-1} multi-element external standard for 15 elements (Cr, Ti, V, Mn, Co, Ni, Cu, Zn, As, Mo, Sn, Sb, Ba, Tl and Pb) was prepared by mixing 10 μg mL^{-1} custom multi-element standard, 1000 μg mL^{-1}Ti, and 1000 μg mL^{-1} Sn and then diluting with 0.1 mol L^{-1} nitric acid. Aerosols of the multi-element external standard generated by the USN were trapped on tandem nitro cellulose filters (pore size, 0.22 μm; MILLEX-LG for ion chromatography, FOS1S0017, Dionex, Japan) for 15 min. Trapped elements were extracted with four 2.5-mL portions of 0.1 mol L^{-1} HNO_3, and then the element concentrations were determined by ICP-MS. We

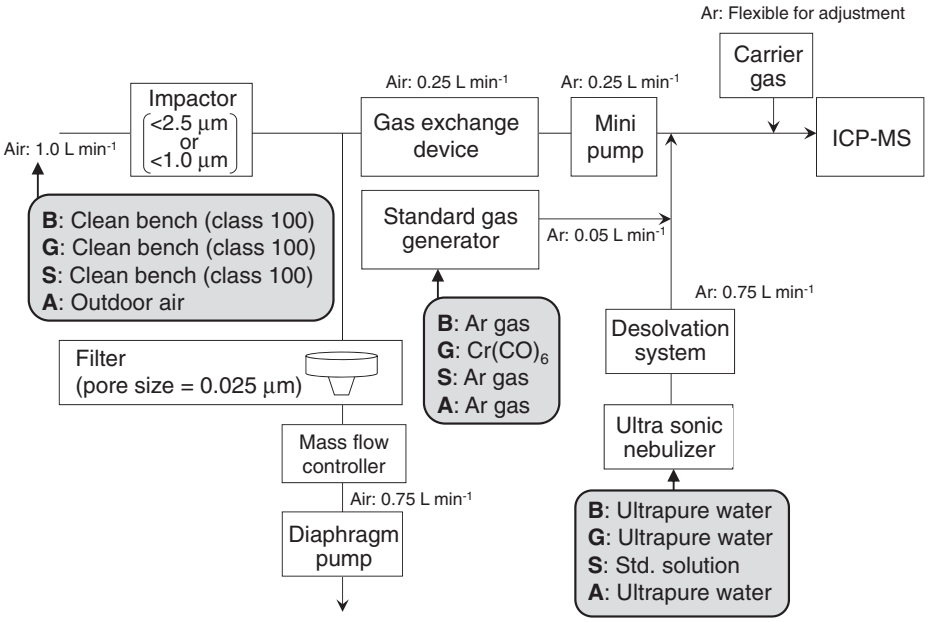

Fig. 1. Schematic diagram of apparatus for real-time analysis. B: blank; G: $Cr(CO)_6$ gas; S: standard solution; and A: outdoor air.

Table 1
ICP-MS operating parameters.

Sampling date	24th Sep, 2010	23rd Sep, 2010	9th Nov, 16th Nov, 12th Dec, and 13th Dec, 2011
Diameter of APs	PM2.5 (<2.5 μm)	PM2.5 (<2.5 μm)	PM1.0 (<1.0 μm)
RF power	1400 W	1400 W	1400 W
Total Ar flow in central torch	1.10–1.15 L min^{-1}	1.10–1.15 L min^{-1}	1.10–1.15 L min^{-1}
Torch	Normal (i.d. = 2.0 mm)	Normal (i.d. = 2.0 mm)	Demountable (i.d. = 4.0 mm)
Sampling depth	7.1 mm	7.1 mm	5.0–6.0 mm
Dwell time	10 ms $point^{-1}$	100 s $point^{-1}$	3 s $point^{-1}$
Data point	1 $point^{-1}$	3 $point^{-1}$	3 $point^{-1}$
Repetition	3000 times	60 times	200 times
Isotope	^{208}Pb	^{208}Pb	^{47}Ti, ^{51}V, ^{53}Cr, ^{55}Mn, ^{59}Co, ^{60}Ni, ^{65}Cu, ^{66}Zn, ^{75}As, ^{95}Mo, ^{118}Sn, ^{121}Sb, ^{137}Ba, ^{205}Tl, ^{208}Pb
Mode	Time resolved	Quantification	Quantification

confirmed the trace element extraction efficiency of this procedure by separate analysis of each extracted solution. The trapping efficiency of the filters (E_t) was calculated with Eq. (2):

$$E_t = \frac{(M_1 - M_2)}{M_1} \times 100\% \quad (2)$$

where M_1 and M_2 are the element masses (ng) collected on filters 1 and 2, respectively.

The sample introduction efficiency of the USN determined by comparison with filter-collection data (E_f) was calculated with Eq. (3):

$$E_f = \frac{M_1 \times 100/E_t}{C \times F_s \times T} \times 100\% = \frac{M_1^2/(M_1 - M_2)}{C \times F_s \times T} \times 100\% \quad (3)$$

where C is the concentration (ng mL^{-1}) of elements in the multi-element external standard solution introduced into the USN; F_s is the uptake rate (mL min^{-1}) of the multi-element external standard solution into the USN; and T is duration (min) of nebulization.

Finally, we compared the E_g and E_f values to validate the method used for calculation of the E_g value for the USN.

2.5. Quantification of elements in APs simultaneously collected on a filter

The APs that were simultaneously collected on a cellulose nitrate filter were acid-digested as described in the literature [1]. HNO_3 (6 mL), HF (3 mL), and H_2O_2 (1 mL) were added to the samples, which were then digested with a microwave digestion system (MLS 1200, Milestone, Italy). After microwave digestion, HF was evaporated by means of a hot plate (230 °C). When the solution was reduced to a single transparent droplet (*ca.* 0.05 mL), it was diluted to 10 mL with ultrapure water. Trace element concentrations in the solution were determined by ICP-MS, and the concentration units of nanograms per milliliter were converted to nanograms per cubic meter by using an air flow of 0.75 L min^{-1}.

2.6. Data analysis

Meteorological data were obtained from the Japan Meteorological Agency [11]. Wind vector data were depicted by means of an Excel add-in written by Hayakari [12].

3. Results and discussion

3.1. Calculation of the USN sample introduction efficiency

As reported previously for studies of solid samples by means of laser ablation-ICP-MS [13,14], element concentrations in dried aerosol solutions can be accurately quantified. However, the sample introduction efficiency for standard solutions must be determined. In this study, we calculated the sample introduction efficiency by two methods (Eqs. (1) and (3)). For Eq. (1), we used C, F_g, F_s, I_s, I_g, and I_b values of 5.0 ng mL^{-1}, 0.109 ng min^{-1}, 1.56 mL min^{-1}, 10.30×10^4 counts, 1.76×10^4 counts, and 0.26×10^4 counts, respectively; and we calculated that the E_g for introduction of Cr via the USN was 9.4 ± 0.7%. Then we converted the Cr concentration (in nanograms per milliliter) in the multi-element standard solution to a mass flow rate (in nanograms per min).

To validate this method for calculating the introduction efficiency, we also determined the sample introduction efficiency by another method, which involved collecting aerosols on filters and then using Eq. (3). By substituting C, M_1, M_2, F_s, and T values of 190 ng mL^{-1}, 415 ng, 0.06 ng, 1.56 mL min^{-1}, and 15 min into the equation, we calculated the E_f of Cr to be 9.3 ± 0.4%, which agreed well with the calculated E_g. In the same way, the E_f values of other elements were calculated (Table 2). Our results suggest that the introduction efficiency of Cr via the USN was similar to the values for other elements and therefore that the sample introduction efficiency of the USN could be calculated with a Cr standard gas and Eq. (1). This calibration method worked well for 15 elements (Ti, V, Cr, Mn, Co, Ni, Cu, Zn, As, Mo, Sn, Sb, Ba, Tl, and Pb). Using the calculated E_g value, we converted the element concentrations (in nanograms per milliliter) in the multi-element standard solution to element mass flow rates (nanograms per min).

3.2. Real-time monitoring of Pb in APs with diameters <2.5 μm

Fig. 2a shows a single measurement of Pb concentrations in APs with diameters <2.5 μm made with an integration time of 10 ms on 24 September 2010, and Fig. 2b shows its histogram. From five

Table 2
Sample introduction efficiencies from USN calculated from element masses which were trapped on the filter.

Element	Sample introduction efficiency (%) (Average ± S.D.*)
Ti	9.4 ± 0.4
V	9.7 ± 0.4
Cr	9.3 ± 0.4
Mn	9.9 ± 0.7
Co	9.0 ± 0.6
Ni	9.0 ± 0.6
Cu	8.8 ± 0.6
Zn	9.2 ± 0.6
As	7.8 ± 0.3
Mo	9.2 ± 0.3
Sn	9.2 ± 0.3
Sb	9.1 ± 0.3
Ba	8.9 ± 0.6
Tl	7.1 ± 0.4
Pb	8.3 ± 0.5

* S.D. was calculated by the measurements of three individual samples.

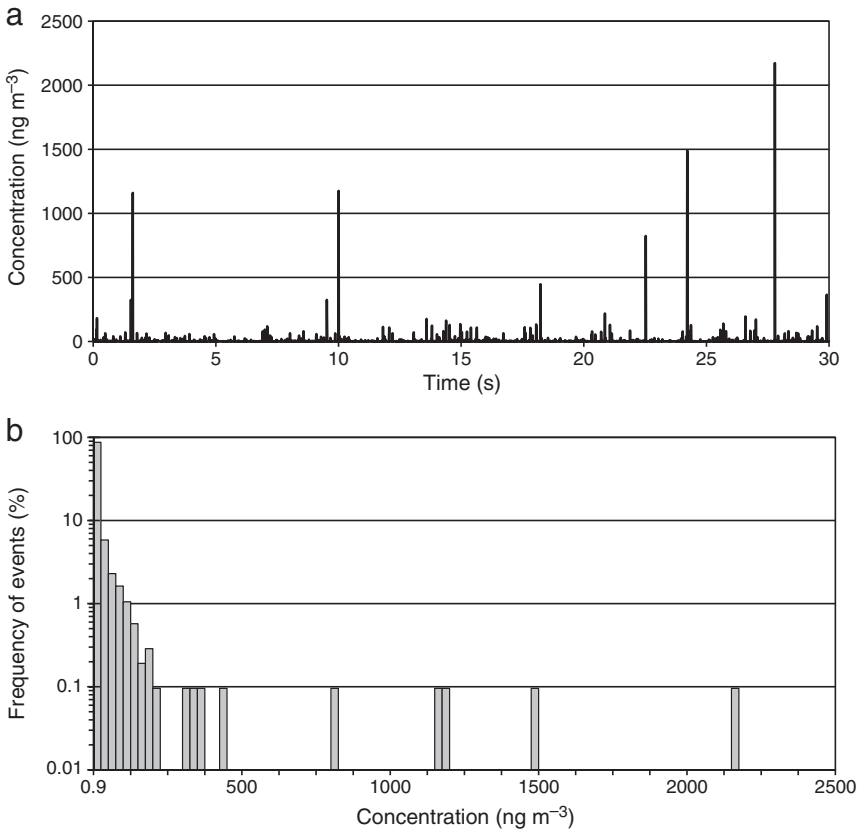

Fig. 2. Real-time monitoring of Pb in APs with diameter <2.5 μm on 24 September 2010 (integration time, 10 ms). (a) A single measurement and (b) relative frequency distribution of detectable events derived from a single measurement.

measurements, the average Pb concentration was 3.9 ± 2.7 ng m^{-3}, which agrees reasonably well with the previously reported average concentration (9.01 ng m^{-3}, our laboratory monitoring data recently obtained) in APs with diameters <2.1 μm collected on a filter over the sampling period of 25 days in September 2011. In Fig. 2a, of all the events, 38.1% were detectable (limit of detection was 0.9 ng m^{-3}) and 14.8% were quantitative (limit of quantification was 3.0 ng m^{-3}). Surprisingly, although 87.2% of the particles showed Pb concentrations from 0.9 to 25 ng m^{-3}, the Pb concentrations in individual particles varied widely, from 0.9 to 2170 ng m^{-3} (Fig. 2b). This result strongly suggests the importance of high-time-resolution analysis of elements in APs.

Fig. 3 shows Pb concentrations in APs with diameters <2.5 μm determined by real-time monitoring for 5 h with an integration time of 5 min on 23 September 2010. The average concentration (0.260 ng m^{-3}) was in good agreement with the concentrations determined for APs collected simultaneously on a filter (0.263 ng m^{-3}). This result indicated that our calibration method worked well for real-time determination of Pb concentrations. Our real-time analysis also showed a significant relationship between Pb concentration and meteorological data. No Pb was detected in APs collected during the period from 14:03 to 15:33 (when it was raining), and the average Pb concentration when the wind blew from the north-northeast (0.35 ng m^{-3}) was higher than the concentrations when the wind blew from other directions (0.17–0.24 ng m^{-3}).

3.3. Real-time multi-element monitoring of APs with diameters <1.0 μm and signal reduction of trace elements

Fig. 4 shows examples of real-time analysis for 15 elements in APs with diameters <1.0 μm collected on 16 November 2011. The Cu and Zn concentrations determined by real-time analysis (0.47 and 0.69 ng m^{-3}) were 1/10 those determined previously for filter-collected APs with diameters <1.2 μm (4.6 and 35.0 ng m^{-3}, respectively) [15]. We simultaneously collected APs on a filter during real-time analysis, and determined elemental recoveries of real-time analysis by comparing with filter-collection data (Table 3). Signals of Ti, Cr, Mn, Ni, Cu, Zn, Sn, and Ba by real-time analysis tended to be lower compared to filter-collection data. These signal reductions indicate that the APs were not completely fused, vaporized, atomized, and ionized in the plasma.

Insufficient fusion or vaporization of particles directly introduced into plasma has been reported previously. Houk and co-workers

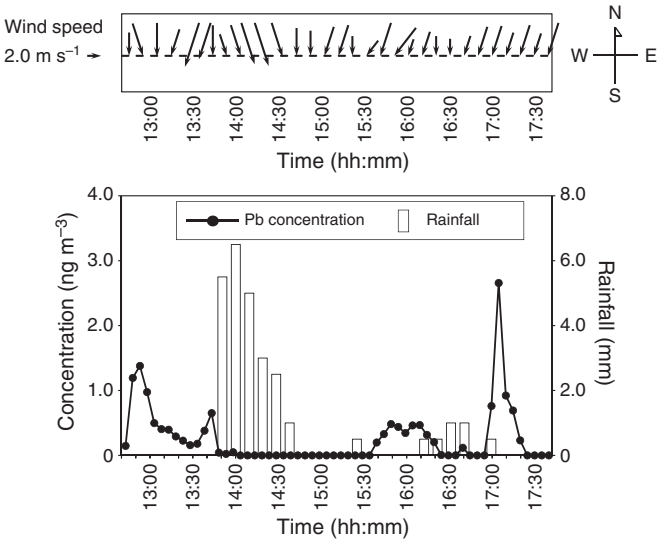

Fig. 3. Real-time monitoring of Pb in APs with diameter <2.5 μm at 5-min intervals on 23 September 2010. (a) Wind vector data and (b) temporal variation of Pb concentration and rainfall amount.

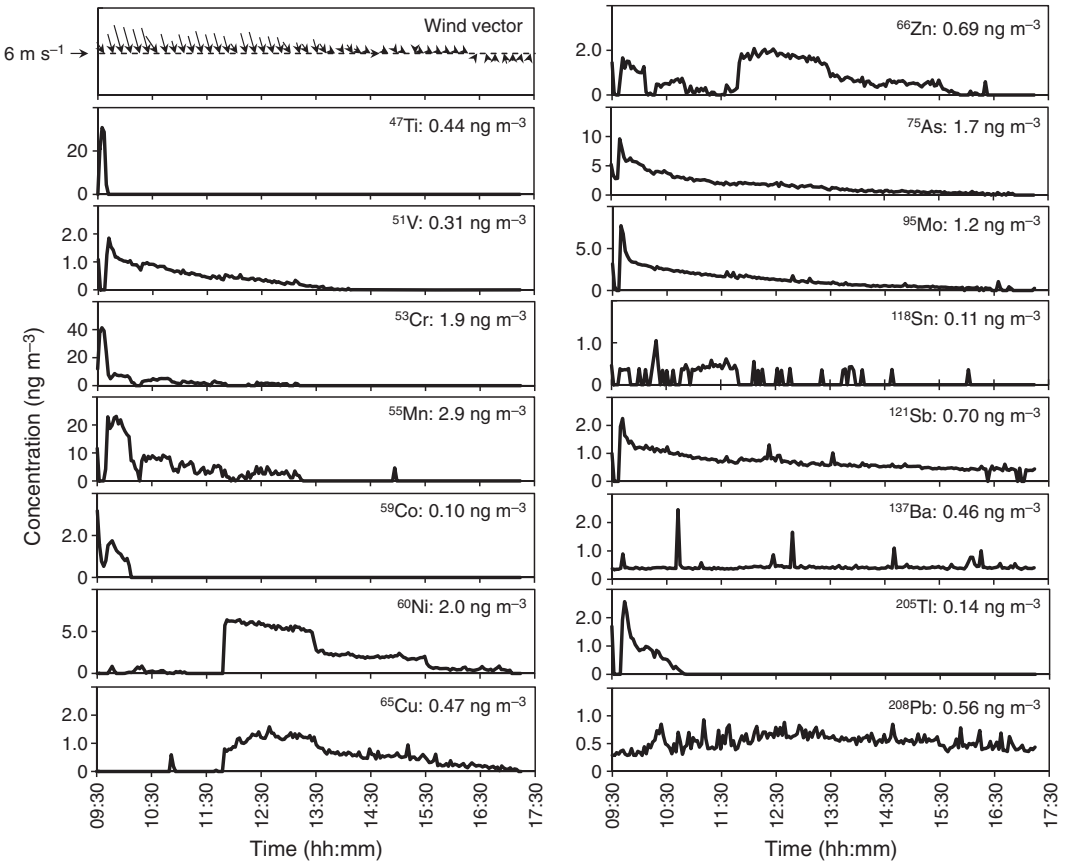

Fig. 4. Real-time monitoring of 15 elements in APs with diameters <1.0 μm at 2.5 min intervals on 16 November 2011, along with wind vector data and the average concentration of each element (upper right of each plot).

[16,17] used high-speed film photography to study the emission behavior of particulates (Y_2O_3 slurry and ablated particles from a Y_2O_3 pellet) and found that these particles produce a noticeable line and a set of discrete tracks along the axis of the plasma. These tracks persist for the entire length of the normal analytical zone, even for particles as small as 1 μm, which suggests that the particles were not fully atomized.

Gunther and co-workers [18–21] used a laser ablation system to generate particles from glass and then studied elemental fractionation, that is, the change in elemental or isotope intensity. They reported that particles with diameters >0.15 μm generated by 266-nm laser ablation of a NIST 610 glass standard were not completely ionized at any plasma power [20,21]. They also reported complete ionization of particles smaller than 90 nm at plasma forward powers of 1000, 1300, and 1600 W.

In air, Sb and Pb in APs with diameters <2.5 μm, whose probable source was fly ash originating from waste incineration, are reported to be distributed mainly in the particle fraction with diameters from 0.5 to 0.7 μm [15]; nevertheless, recoveries of Sb and Pb were relatively good (80 ± 10 and 88 ± 28%, respectively). It was reasonable to expect that the ionization efficiency of elements in a particle should be particle-size dependent. However, from these findings, it

Table 3
Recovery of elements determined by real-time analysis compared with filter- collection data.

Element	Recovery (%) (Average ± S.D.*)
Ti	9.6 ± 10.0
V	89 ± 43
Cr	43 ± 13
Mn	35 ± 50
Co	115 ± 20
Ni	35 ± 36
Cu	20 ± 12
Zn	19 ± 13
As	81 ± 35
Mo	130 ± 59
Sn	14 ± 18
Sb	80 ± 10
Ba	12 ± 8
Tl	60 ± 16
Pb	88 ± 28

* S.D. was calculated by the measurements of three individual samples.

Table 4
Melting and boiling points (°C) of metals and their oxides.*,**.

	Metal		Oxide		
	Melting point	Boiling point		Melting point	Boiling point
Ti	1670	3287	TiO_2	1843	
V	1910	3407	V_2O_5	670	1800_{dec}
Cr	1907	2671	Cr_2O_3	2329	≈3000
Mn	1246	2061	MnO	1839	–
Co	1495	2927	Co_2O_3	895_{dec}	
Ni	1455	2913	NiO	1955	–
Cu	1085	2562	CuO	1446	
Zn	420	907	ZnO	1974	
As	817	614	As_2O_3	313	465
Mo	2623	4639	MoO_3	801	1155
Sn	232	2602	SnO_2	1630	
Sb	631	1587	Sb_2O_3	655	1425
Ba	727	1897	BaO	1972	
Tl	304	1473	Tl_2O_3	834	
Pb	327	1749	PbO	897	

* Melting and boiling points are referenced from Linde2005 [22].
** dec means decomposition.

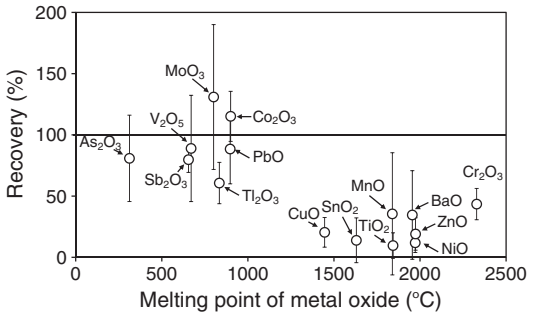

Fig. 5. Correlation between the recoveries of trace elements and the melting points of their oxides. Recoveries were calculated by comparing the concentrations determined by real-time analysis of APs with diameters <1.0 μm and concentrations determined by means of collection on a filter. Error bars indicate standard deviation ($n=4$).

is difficult to conclude whether or not incomplete fusion or vaporization of particles was due to their aerometric diameter.

To clarify the mechanisms of signal reduction for trace elements in APs introduced into the ICP, we compared the melting and boiling points of the elements in their metallic states (Table 4) [22]. Some low-melting and low-boiling metals, such as Zn (mp 420 °C, bp 907 °C) and Sn (mp 202 °C), showed low recoveries; whereas Mo, which has high melting and boiling points (2623 and 4639 °C, respectively) showed relatively good recovery. Fig. 5 shows the relationship between the recoveries of elements in APs with diameters <1.0 μm (average ± standard deviation, $n=4$, data collected on 9 and 16 November and 12 and 13 December 2011) and the melting points of the corresponding oxides [22]. Recovery decreased with increasing oxide melting point, and Pearson's correlation test showed a significant negative correlation between recovery and melting point (-0.775, $p<0.01$). The real-time data and the filter-collection data showed good agreement for elements with low-melting oxides (such as V, Co, As, Mo, Sb, Tl, and Pb). In contrast, the real-time concentrations were lower than the filter-collection concentrations for elements with high-melting oxides (such as Ti, Cr, Mn, Ni, Cu, Zn, Sn and Ba). These results imply that the oxides of Ti, Cr, Mn, Ni, Cu, Zn, Sn and Ba were not completely fused, vaporized, atomized, and ionized in the initial radiation zone of the ICP. Recently, signal reduction for high-melting metal oxides was reported for aerosols generated by laser ablation of NIST SRM 610 [23,24]. This report supports our hypothesis that incomplete fusion or evaporation of metal oxides was responsible for the signal reduction. In addition to melting point of metal oxides, it was also considered that the release of elements from particles by plasma depends on the spatial distribution of elements in a particle. Large error bar might indicate the differences in depth profile of elements.

3.4. Application of real-time monitoring data to partitioning sources

Because some elements with high-melting oxides showed signal reduction in APs with diameters <1 μm, the measured concentrations must be corrected for recovery prior to quantitative statistical analysis. Fig. 6 shows average concentrations of trace elements according to wind direction after correction for the element recovery. V, Co, Ni, Cu, Zn, and Ba concentrations were higher when the winds were southwesterly to southeasterly than when the wind blew from other directions. Cr, Mn, Sn, As, and Tl concentrations were higher when the winds were northwesterly to northeasterly. Ti, Sb, and Pb concentrations were high when winds were northerly or southerly. In particular, higher concentrations of V (which showed good recovery) and Ni (which showed poor recovery) were observed during southerly and southeasterly winds.

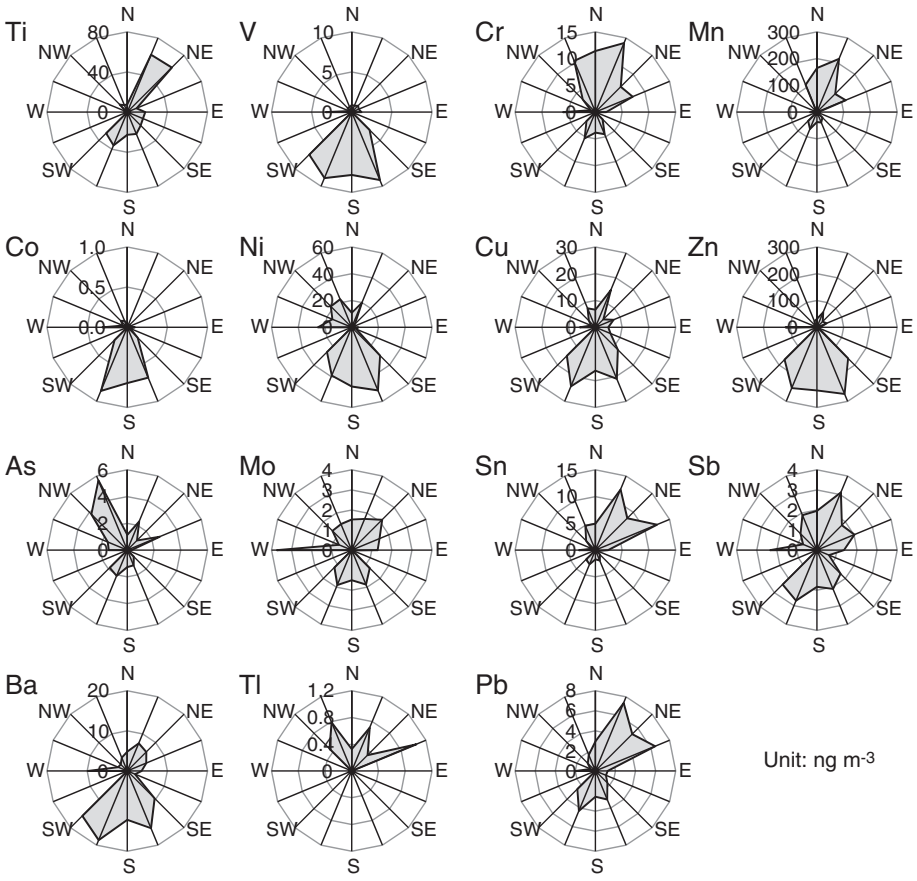

Fig. 6. Wind direction profiles of trace element concentrations in APs with diameters <1.0 μm obtained by real-time analysis, after correction for recoveries calculated from filter-collection data obtained simultaneously. Samplings were performed on 9 and 16 November and 12 and 13 December 2011.

These trends are similar to previously reported trends. It has been reported that V and Ni concentrations in APs with diameters <2 μm are high in Tokyo during summer (from June to August) [1], when the prevailing wind carries particles from the southeast to the northwest. These elements are released during combustion of fossil fuel, and it is suspected that they are emitted from industrial facilities located along the coastline of Tokyo Bay. As given in the supplementary data (Fig. A), different trends could be observed without correction for the element recovery. These findings suggested that quantifiable environmental monitoring data can be obtained by real-time analysis after correction for the element recovery. However, recoveries of element were influenced by spatial distribution of elements in a particle, as well as melting point of metal oxide. High RF power (1600 W), low carrier gas flow, and long sampling depth might be useful for sufficient fusion/vaporization/ionization of particles.

4. Conclusions

A new calibration system for real-time analysis of trace elements in APs was developed. Our calibration method with a USN worked well for 15 elements (Ti, V, Cr, Mn, Co, Ni, Cu, Zn, As, Mo, Sn, Sb, Ba, Tl and Pb) after correction for sample introduction efficiency, which was calculated by comparing Cr intensities of a standard solution introduced via the USN and with the Cr intensity for a $Cr(CO)_6$ standard gas introduced by means of a standard gas generator. The E_g value for Cr was the same as the E_f values for Cr and the other 14 elements. The real-time data and the filter-collection data agreed well for elements with low-melting oxides (e.g., V, Co, As, Mo, Sb, Tl, and Pb). In contrast, the real-time data were lower than the filter-collection data for elements with high-melting oxides (e.g., Ti, Cr, Mn, Ni, Cu, Zn, Sn and Ba). This result implies that Ti, Cr, Mn, Ni, Cu, Zn, Sn and Ba oxides were not completely fused, vaporized, atomized, and ionized in the ICP. However, quantitative real-time analysis could be performed as long as the real-time data were corrected for the element recoveries determined by simultaneous collection on a filter.

Acknowledgments

We acknowledge Mr. Kohei Nishiguchi and Mr. Keisuke Utani (J-Science Lab. Co.) for their support and invaluable comments. This research was supported by a grant-in-aid from the Ministry of Education, Culture, Sports, Science and Technology, Japan (no. 2255 0081). Part of this study was supported by the joint research project entitled "Development of single particle measurement system for the determination of trace elements in size-classified nanoparticles."

Appendix A. Supplementary data

Supplementary data to this article can be found online at http://dx.doi.org/10.1016/j.sab.2012.06.001.

References

[1] N. Furuta, A. Iijima, A. Kambe, K. Sakai, K. Sato, Concentrations, enrichment and predominant sources of Sb and other trace elements in size classified airborne particulate matter collected in Tokyo from 1995 to 2004, J. Environ. Monit. 7 (2005) 1155–1161.
[2] Y. Suzuki, T. Suzuki, N. Furuta, Determination of rare earth elements (REEs) in airborne particulate matter (APM) collected in Tokyo, Japan, and a positive anomaly of europium and terbium, Anal. Sci. 26 (2010) 929–935.
[3] Y. Suzuki, S. Hikida, N. Furuta, Cycling of rare earth elements in the atmosphere in central Tokyo, J. Environ. Monit. 13 (2011) 3420–3428.
[4] S. Kaneco, T. Nomizu, T. Tanaka, N. Mizutani, H. Kawaguchi, Optimization of operating-conditions in individual airborne particle analysis by inductively-coupled plasma-mass spectrometry, Anal. Sci. 11 (1995) 835–840.
[5] H. Kawaguchi, N. Fukasawa, A. Mizuike, Investigation of airborne particles by inductively coupled plasma emission-spectrometry calibrated with monodisperse aerosols, Spectrochim. Acta Part B 41 (1986) 1277–1286.
[6] T. Nomizu, H. Hayashi, N. Hoshino, T. Tanaka, H. Kawaguchi, K. Kitagawa, S. Kaneco, Determination of zinc in individual airborne particles by inductively coupled plasma mass spectrometry with digital signal processing, J. Anal. At. Spectrom. 17 (2002) 592–595.
[7] T. Nomizu, S. Kaneco, T. Tanaka, T. Yamamoto, H. Kawaguchi, Determination of femto-gram amounts of zinc and lead in individual airborne particles by inductively-coupled plasma-mass spectrometry with direct air-sample introduction, Anal. Sci. 9 (1993) 843–846.
[8] T. Myojo, M. Takaya, M. Ono-Ogasawara, DMA as a gas converter from aerosol to "argonsol" for real-time chemical analysis using ICP-MS, Aerosol Sci. Technol. 36 (2002) 76–83.
[9] K. Nishiguchi, K. Utani, E. Fujimori, Real-time multielement monitoring of airborne particulate matter using ICP-MS instrument equipped with gas converter apparatus, J. Anal. At. Spectrom. 23 (2008) 1125–1129.
[10] Y. Suzuki, H. Sato, S. Hikida, K. Nishiguchi, N. Furuta, Real-time monitoring and determination of Pb in a single airborne nanoparticle, J. Anal. At. Spectrom. 25 (2010) 947–949.
[11] Japan Meteorological Agency, Forepast meteorological database, http://www.data.jma.go.jp/obd/stats/etrn/index.php, 2012.
[12] S. Hayakari, Excel® addin for meteorological data, http://www.jomon.ne.jp/~hayakari/index.html.
[13] J.S. Becker, C. Pickhardt, H.J. Dietze, Determination of trace elements in high-purity platinum by laser ablation inductively coupled plasma mass spectrometry using solution calibration, J. Anal. At. Spectrom. 16 (2001) 603–606.
[14] J.J. Leach, L.A. Allen, D.B. Aeschliman, R.S. Houk, Calibration of laser ablation inductively coupled plasma mass spectrometry using standard additions with dried solution aerosols, Anal. Chem. 71 (1999) 440–445.
[15] A. Iijima, K. Sato, Y. Fujitani, E. Fujimori, Y. Saito, K. Tanabe, T. Ohara, K. Kozawa, N. Furuta, Clarification of the predominant emission sources of antimony in airborne particulate matter and estimation of their effects on the atmosphere in Japan, Environ. Chem. 6 (2009) 122–132.
[16] R.S. Houk, R.K. Winge, X.S. Chen, High speed photographic study of wet droplets and solid particles in the inductively coupled plasma, J. Anal. At. Spectrom. 12 (1997) 1139–1148.
[17] D.B. Aeschliman, S.J. Bajic, D.P. Baldwin, R.S. Houk, High-speed digital photographic study of an inductively coupled plasma during laser ablation: comparison of dried solution aerosols from a microconcentric nebulizer and solid particles from laser ablation, J. Anal. At. Spectrom. 18 (2003) 1008–1014.
[18] M. Guillong, D. Gunther, Effect of particle size distribution on ICP-induced elemental fractionation in laser ablation-inductively coupled plasma-mass spectrometry, J. Anal. At. Spectrom. 17 (2002) 831–837.
[19] M. Guillong, H.R. Kuhn, D. Gunther, Application of a particle separation device to reduce inductively coupled plasma-enhanced elemental fractionation in laser ablation-inductively coupled plasma-mass spectrometry, Spectrochim Acta Part B 58 (2003) 211–220.
[20] H.R. Kuhn, M. Guillong, D. Gunther, Size-related vaporisation and ionisation of laser-induced glass particles in the inductively coupled plasma, Anal. Bioanal. Chem. 378 (2004) 1069–1074.
[21] H.R. Kuhn, D. Gunther, Laser ablation-ICP-MS: particle size dependent elemental composition studies on filter-collected and online measured aerosols from glass, J. Anal. At. Spectrom. 19 (2004) 1158–1164.
[22] D.R. Lide (Ed.), CRC Handbook of Chemistry and Physics, 86th ed., Taylor & Francis, 2005.
[23] R. Brogioli, B. Hattendorf, J. Koch, H. Wiltsche, L. Flamigni, D. Gunther, Online electrothermal heating of laser-generated aerosols: effects on aerosol particle size and signal intensities in ICPMS, Anal. Bioanal. Chem. 399 (2011) 2201–2209.
[24] L. Flamigni, J. Koch, H. Wiltsche, R. Brogioli, S. Gschwind, D. Gunther, Visualization, velocimetry, and mass spectrometric analysis of engineered and lase-produced particles passing through inductively coupled plasma sources, J. Anal. At. Spectrom. 27 (2012) 619–625.